

# Quantum many-body dynamics in optomechanical arrays

Max Ludwig<sup>1,\*</sup> and Florian Marquardt<sup>1,2</sup>

<sup>1</sup>*Institute for Theoretical Physics, Universität Erlangen-Nürnberg, Staudtstraße 7, 91058 Erlangen, Germany*

<sup>2</sup>*Max-Planck-Institute for the Science of Light, Günther-Scharowsky-Straße 1/Bau 24, 91058 Erlangen, Germany*

We study the nonlinear driven dissipative quantum dynamics of an array of optomechanical systems. At each site of such an array, a localized mechanical mode interacts with a laser-driven cavity mode via radiation pressure, and both photons and phonons can hop between neighboring sites. The competition between coherent interaction and dissipation gives rise to a rich phase diagram characterizing the optical and mechanical many-body states. For weak intercellular coupling, the mechanical motion at different sites is incoherent due to the influence of quantum noise. When increasing the coupling strength, however, we observe a transition towards a regime of phase-coherent mechanical oscillations. We employ a Gutzwiller ansatz as well as semiclassical Langevin equations on finite lattices, and we propose a realistic experimental implementation in optomechanical crystals.

*Introduction.* - Recent experimental progress has brought optomechanical systems into the quantum regime: A single mechanical mode interacting with a laser-driven cavity field has been cooled to the ground state [14, 17]. Several of these setups, in particular optomechanical crystals, offer the potential to be scaled up to form optomechanical arrays. Applications of such arrays for quantum information processing [3, 4] have been proposed. Given these developments, one is led to explore quantum many-body effects in optomechanical arrays. In this work, we analyze the nonlinear photon and phonon dynamics in a homogeneous two-dimensional optomechanical array. In contrast to earlier works [3–6], here we study the array’s quantum dynamics beyond a quadratic Hamiltonian. To tackle the non-equilibrium many-body problem of this nonlinear dissipative system, we employ a mean-field approach for the collective dynamics. First, we discuss photon statistics in the array, in particular how the photon blockade effect [7] is altered in the presence of intercellular coupling. The main part of the article focuses on the transition of the collective mechanical motion from an incoherent state (due to quantum noise) to an ordered state with phase-coherent mechanical oscillations. For these dynamics, the dissipative effects induced by the optical modes play a crucial role. On the one hand, they allow the mechanical modes to settle into self-induced oscillations [8] once the optomechanical amplification rate exceeds the intrinsic mechanical damping. On the other hand, the fundamental quantum noise (e.g. cavity shot noise) diffuses the mechanical phases and prevents the mechanical modes from synchronizing. This interplay leads to an elaborate phase diagram characterizing the transition. We develop a semiclassical model to describe the effective dynamics of the mechanical phases and to study the system on finite lattices.

While true long-range order is prohibited for a two-dimensional system with continuous symmetry, at least for equilibrium systems, a Beresinskii-Kosterlitz-Thouless transition towards a state with quasi-long-range order is possible. The ordered mechanical phase thus

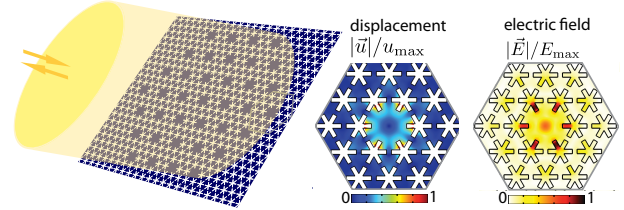


Figure 1. Example implementation of an optomechanical array: A two-dimensional snowflake optomechanical crystal [18, 20] supports localized optical and mechanical modes around defect cavities. Here, we propose arranging them in a super structure, forming the array. The insets show electric field  $\vec{E}$  and displacement field  $\vec{u}$  of an isolated defect cavity (obtained from finite element simulations). Due to the finite overlap between modes of neighboring sites [29], photons and phonons can hop through the array, see Eq. (2). A wide laser beam drives the optical modes of the array continuously and the reflected light is read out.

resembles the superfluid phase in two-dimensional cold atomic gases [9] or Josephson junction arrays [10]. Notably, optomechanical arrays combine the tunability of optical systems with the robustness and durability of an integrated solid-state device. Other driven dissipative systems that have been studied with regard to phase transitions recently include cold atomic gases [11–14], nonlinear cavity arrays [15, 16] and optical fibers [17]. In a very recent work and along the lines of [11], the preparation of long-range order for photonic modes was proposed using the linear dissipative effects in an optomechanical array [5]. Our work adds the novel aspect of a mechanical transition to the studies of driven dissipative many-body systems.

*Model.* - We study the collective quantum dynamics of a two-dimensional homogeneous array of optomechanical cells (Fig. 1). Each of these cells consists of a mechanical mode and a laser driven optical mode that interact via

the radiation pressure coupling at a rate  $g_0$  ( $\hbar = 1$ ):

$$\hat{H}_{\text{om},j} = -\Delta \hat{a}_j^\dagger \hat{a}_j + \Omega \hat{b}_j^\dagger \hat{b}_j - g_0 (\hat{b}_j^\dagger + \hat{b}_j) \hat{a}_j^\dagger \hat{a}_j + \alpha_L (\hat{a}_j^\dagger + \hat{a}_j). \quad (1)$$

The mechanical mode ( $\hat{b}_j$ ) is characterized by a frequency  $\Omega$ . The cavity mode ( $\hat{a}_j$ ) is transformed into the frame rotating at the laser frequency ( $\Delta = \omega_{\text{laser}} - \omega_{\text{cav}}$ ) and driven at the rate  $\alpha_L$ . In the most general case, both photons and phonons can tunnel between neighboring sites ( $\langle ij \rangle$ ) at rates  $J/z$  and  $K/z$ , where  $z$  denotes the coordination number. The full Hamiltonian of the array is given by  $\hat{H} = \sum_j \hat{H}_{\text{om},j} + \hat{H}_{\text{int}}$ , with

$$\hat{H}_{\text{int}} = -\frac{J}{z} \sum_{\langle i,j \rangle} (\hat{a}_i^\dagger \hat{a}_j + \hat{a}_i \hat{a}_j^\dagger) - \frac{K}{z} \sum_{\langle i,j \rangle} (\hat{b}_i^\dagger \hat{b}_j + \hat{b}_i \hat{b}_j^\dagger) \quad (2)$$

To bring this many-body problem into a treatable form, we apply the Gutzwiller ansatz  $\hat{A}_i^\dagger \hat{A}_j \approx \langle \hat{A}_i^\dagger \rangle \hat{A}_j + \hat{A}_i^\dagger \langle \hat{A}_j \rangle - \langle \hat{A}_i^\dagger \rangle \langle \hat{A}_j \rangle$  to Eq. (2). The accuracy of this approximation improves if the number of neighboring sites  $z$  increases. For identical cells, the index  $j$  can be dropped and the Hamiltonian reduces to a sum of independent contributions, each of which is described by

$$\hat{H}_{\text{mf}} = \hat{H}_{\text{om}} - J(\hat{a}^\dagger \langle \hat{a} \rangle + \hat{a} \langle \hat{a}^\dagger \rangle) - K(\hat{b}^\dagger \langle \hat{b} \rangle + \hat{b} \langle \hat{b}^\dagger \rangle). \quad (3)$$

Hence, a Lindblad master equation for the single cell density matrix  $\hat{\rho}$ ,  $d\hat{\rho}/dt = -i[\hat{H}_{\text{mf}}, \hat{\rho}] + \kappa \mathcal{D}[\hat{a}]\hat{\rho} + \Gamma \mathcal{D}[\hat{b}]\hat{\rho}$  can be employed. The Lindblad terms  $\mathcal{D}[\hat{A}]\hat{\rho} = \hat{A}\hat{\rho}\hat{A}^\dagger - \hat{A}^\dagger\hat{A}\hat{\rho}/2 - \hat{\rho}\hat{A}^\dagger\hat{A}/2$  take into account photon decay at a rate  $\kappa$  and mechanical dissipation (here assumed due to a zero temperature bath) at a rate  $\Gamma$ .

*Photon statistics.* - Recently, it was shown that the effect of photon blockade [7] can appear in a single optomechanical cell: The interaction with the mechanical mode induces an optical nonlinearity of strength  $g_0^2/\Omega$  [7, 18] and the presence of a single photon can hinder other photons from entering the cavity. To observe this effect, the nonlinearity must be comparable to the cavity decay rate, i.e.  $g_0^2/\Omega \gtrsim \kappa$ , and the laser drive weak ( $\alpha_L \ll \kappa$ ) [7, 19].

To study nonclassical effects in the photon statistics, we analyze the steady-state photon correlation function  $g^{(2)}(\tau) = \langle \hat{a}^\dagger(t) \hat{a}^\dagger(t+\tau) \hat{a}(t+\tau) \hat{a}(t) \rangle / \langle \hat{a}^\dagger(t) \hat{a}(t) \rangle^2$  [20] at equal times ( $\tau = 0$ ). Here (Fig. 2), we probe the influence of the collective dynamics by varying the optical coupling strength  $J$ , while keeping the mechanical coupling  $K$  zero for clarity. We note that, when increasing  $J$ , the optical resonance effectively shifts:  $\Delta \rightarrow \Delta + J$ . To keep the photon number fixed while increasing  $J$ , the detuning has to be adapted [21]. In this setting, we observe that the interaction between the cells suppresses anti-bunching (Fig. 2 (b)). Photon blockade is lost if the intercellular coupling becomes larger than the effective nonlinearity,  $2J \gtrsim g_0^2/\Omega$ . Above this value, the photon

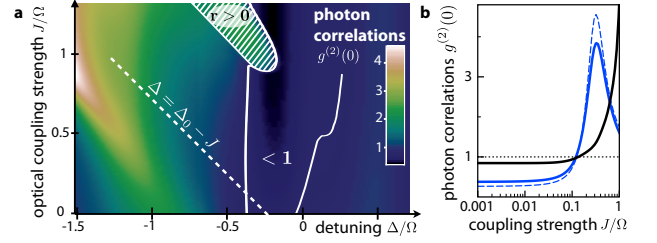


Figure 2. Loss of photon blockade for increasing optical coupling in an array of optomechanical cavities. (a) The equal time photon correlation function shows anti-bunching ( $g^{(2)}(0) < 1$ ) and bunching ( $g^{(2)}(0) > 1$ ) as a function of detuning  $\Delta$  and optical coupling strength  $J$ . The smallest values of  $g^{(2)}(0)$  are found for a detuning  $\Delta_0 = -g_0^2/\Omega$ . (b) When increasing the coupling  $J$  while keeping the intracavity photon number constant, i.e. along the dashed line in panel (a), photon blockade is lost (black solid line). For a smaller driving power (blue solid line,  $\alpha_L = 5 \cdot 10^{-5} \kappa$ ), anti-bunching is more pronounced and the behavior is comparable to that of a nonlinear cavity (dashed line). The hatched area in (a) outlines a region where a transition towards coherent mechanical oscillations has set in.  $\kappa = 0.3 \Omega$ ,  $\alpha_L = 0.65 \kappa$ ,  $g_0 = 0.5 \Omega$ ,  $\Gamma = 0.074 \Omega$ .

statistics shows bunching, and ultimately reaches Poissonian statistics for large couplings. Similar physics has recently been analyzed for coupled qubit-cavity arrays, [21]. For large coupling strengths, though, Fig. 2(a) reveals signs of the collective mechanical motion (hatched area). There we observe the correlation function to oscillate (at the mechanical frequency) and to show bunching. We will now investigate this effect.

*Collective mechanical quantum effects.* - To describe the collective mechanical motion of the array, we focus on the case of purely mechanical intercellular coupling ( $K > 0$ ,  $J = 0$ ) for simplicity. Note, though, that the effect is also observable for optically coupled arrays, as discussed above.

As our main result, Figs. 3(a) and (d) show the sharp transition between incoherent self-oscillations and a phase-coherent collective mechanical state as a function of both laser detuning  $\Delta$  and coupling strength  $K$ : In the regime of self-induced oscillations, the phonon number  $\langle \hat{b}^\dagger \hat{b} \rangle$  reaches a finite value. Yet, the expectation value  $\langle \hat{b} \rangle$  remains small and constant in time. When increasing the intercellular coupling, though,  $\langle \hat{b} \rangle$  suddenly starts oscillating and reaches a steady state

$$\langle \hat{b} \rangle(t) = \bar{b} + r e^{-i\Omega_{\text{eff}} t}. \quad (4)$$

Here, we introduced the mechanical coherence  $r$  and the oscillation frequency  $\Omega_{\text{eff}}$ , which is shifted by the optical fields and the intercellular coupling, cf. Eq. (S.11).

Our more detailed analysis (see below) indicates that this transition results from the competition between the fundamental quantum noise of the system and the ten-

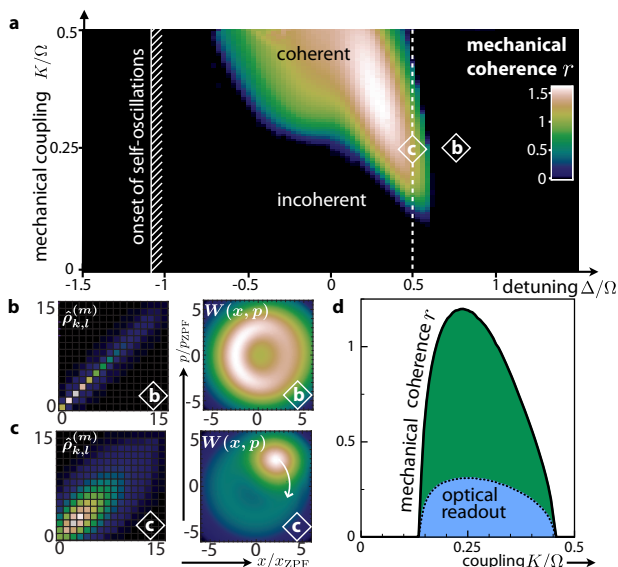


Figure 3. Transition from the incoherent to the synchronized (coherent) phase: (a) Mechanical coherence  $r$  (Eq. (4)) as a function of laser detuning  $\Delta$  and mechanical coupling  $K$ . At weak coupling, the self-oscillations are incoherent,  $r = 0$ , due to quantum noise. When increasing the coupling strength, the systems shows a sharp transition towards the ordered regime, where the mechanical oscillations are phase-coherent,  $r > 0$ . (b,c) Modulus of the density matrix elements (in Fock space) and Wigner density of the collective mechanical state in the incoherent (b) and the coherent regime (c), as marked in (a). (d) Mechanical coherence  $r$  as a function of coupling strength  $K$  along the dashed line in (a). The dotted line shows the optical readout of coherence, i.e. the oscillating component of the photon number  $\langle \hat{a}^\dagger \hat{a} \rangle$ , proportional to the intensity of the reflected beam and thus directly accessible in experiment.  $g_0 = \kappa = 0.3\Omega$ ,  $\alpha_L = 1.1\kappa$ ,  $\Gamma = 0.074\Omega$

density of phase locking between the coupled nonlinear oscillators. Below threshold, the quantum noise from the phonon bath and the optical fields diffuses the mechanical phases at different sites and drives the mechanical motion into an incoherent mixed state. The reduced density matrix  $\hat{\rho}^{(m)}$  is predominantly occupied on the diagonal, see Fig. 3(b), and the Wigner distribution,  $W(x, p) = \frac{1}{\pi\hbar} \int_{-\infty}^{\infty} \langle x-y | \hat{\rho}^{(m)} | x+y \rangle e^{2ipy/\hbar} dy$ , has a ring-like shape, reflecting the fact that the mechanical phase is undetermined [22, 23]. Above threshold, the mechanical motion at different sites becomes phase locked, and the coherence parameter  $r$  reaches a finite value. The emergence of coherence also becomes apparent from the off-diagonal elements of  $\hat{\rho}^{(m)}$  (Fig. 3(c)). The corresponding Wigner function assumes the shape of a coherent state with a definite phase oscillating in phase space. Thus, this transition spontaneously breaks the time-translation symmetry. In a two-dimensional implementation, true long-range order is excluded, but the coherence between different sites is expected to decay as a power law with distance. We also note that this tran-

sition is the quantum mechanical analogon of classical synchronization, which was studied for optomechanical systems in [1, 8, 25]. An important difference is, though, that the classical nonlinear dynamics was analyzed for an inhomogeneous (with disordered mechanical frequencies) system in the absence of noise [1, 8, 25], while in our case disorder is only introduced via fundamental quantum noise. Quantum synchronization has also been discussed in the context of linear oscillators [27] and nonlinear cavities [28] recently.

The laser detuning determines both the strength of the self-oscillations and the influence of the cavity shot noise on the mechanical motion. It turns out that the diffusion of the mechanical phases is pronounced close to the onset of self-oscillations and at the mechanical sideband [29]. As we will show below, even the coherent coupling between the mechanical phases (ultimately leading to synchronization) is tunable via the laser frequency. As a result, the synchronization threshold depends non-trivially on the detuning parameter  $\Delta$ , see Fig. 3(a).

*Langevin dynamics on finite lattices.* - In order to gain further insight into the coupling and decoherence mechanisms as well as effects of geometry and dimensionality, we analyze the semi-classical Langevin equations of the full optomechanical array:

$$\begin{aligned} \dot{\beta}_i &= \left(-i\Omega - \frac{\Gamma}{2}\right)\beta_i + ig_0|\alpha_i|^2 + i\frac{K}{z} \sum_{\langle ij \rangle} \beta_j + \sqrt{\frac{\Gamma}{2}}\xi_{\beta} \\ \dot{\alpha}_i &= \left(i\Delta + ig_0(\beta_i + \beta_i^*) - \frac{\kappa}{2}\right)\alpha_i - i\alpha_L + \sqrt{\frac{\kappa}{2}}\xi_{\alpha}. \end{aligned} \quad (5)$$

The fluctuating noise forces  $\xi_{\sigma=\alpha,\beta}(t)$  mimic the effects of the zero temperature phonon bath and the cavity shot noise, respectively. They are independent at each site and obey  $\langle \xi_{\sigma} \rangle = 0$  and  $\langle \xi_{\sigma}(t)\xi_{\sigma}^*(t') \rangle = \delta(t-t')$ . In this context,  $\langle \dots \rangle$  denotes the average over different realizations of the stochastic terms. This Langevin approach is equivalent to the truncated Wigner approximation (see [30] for a review), and it has shown good qualitative agreement with the full quantum dynamics for a single optomechanical cell [2, 22]. It allows us to treat the effects of quantum fluctuations at all wavelengths on the spatial phase correlations via numerical simulations. At this point, a full quantum treatment for sufficiently large systems remains a challenging problem for future studies.

First, we study the onset of quasi-long-range order in a finite system. To this end we evaluate the correlations  $C(d = |i-j|) = \langle e^{i\varphi_i} e^{-i\varphi_j} \rangle$ , where  $e^{i\varphi_i} = \beta_i/|\beta_i|$ . Numerical calculations on a  $30 \times 30$  square lattice (see Fig. 4(a)) indicate that for weak intercellular coupling the mechanical phases at different sites are uncorrelated even for small distances  $d$ . When increasing the coupling strength, however, the mechanical motion becomes correlated over the whole array with only a slow decrease with distance. The coupling threshold, here defined by setting a lower bound of  $C(14) > 0.01$ , varies with cor-

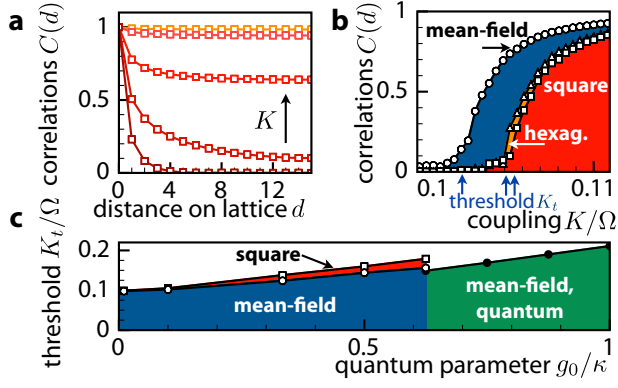


Figure 4. Langevin dynamics on finite lattices: (a) Correlations  $C(d = |i - j|) = |\langle e^{i\varphi_i} e^{-i\varphi_j} \rangle|$  in a  $30 \times 30$  optomechanical array. Quasi-long-range order sets in for sufficiently large coupling strengths.  $K = \{0.09, 0.105, 0.107, 0.12, 0.15\}\Omega$  (b) Correlations over a distance of  $d = 14$  as a function of mechanical coupling strength  $K$  for a square lattice ( $z = 4$ , squares), a hexagonal lattice ( $z = 6$ , triangles) slightly below the mean-field result (circles). (c) Coupling threshold as a function of quantum parameter  $g_0/\kappa$  (squares: square lattice, empty (filled) circles: semi-classical (quantum) mean-field approach).  $\Delta + g_0^2/\Omega = 0.34$ ,  $g_0 = 0.1\kappa$  in (a),(b),  $g_0\alpha_L = 0.33\kappa$  in (c), other parameters as in Fig. 3.

dination number, see Fig. 4(b). Within the mean-field approximation, i.e. for a lattice with global coupling of all sites, fluctuations between neighboring sites and hence the threshold value are underestimated. The coupling threshold grows with the quantum parameter [22], i.e. the ratio of optomechanical coupling and cavity decay rate,  $g_0/\kappa$ , see Fig. 4(c): For  $g_0 \approx \kappa$ , single photons and phonons interact strongly and quantum fluctuations hamper synchronization.

*Synchronization threshold.* - For an analytical approach, the complexity of the Langevin equations can be reduced by integrating out the dynamics of the optical modes and the mechanical amplitudes and by going back to the mean-field approximation [29]. The resulting equation describes the coupling of the mechanical phase on a single site,  $\varphi$ , to a mean field  $\Psi$ :

$$\dot{\varphi} = -\Omega(\bar{A}) + KR \cos(\Psi - \varphi) + K_1 R \sin(\Psi - \varphi) + \sqrt{2D_\varphi} \xi_\varphi + \mathcal{O}(R^2). \quad (6)$$

Here, the order parameter is defined as  $\langle e^{i\varphi_j} \rangle \equiv Re^{i\Psi}$ . The rate  $K_1 = (d\Omega - K/2)K/\gamma$  determines the coupling of phases mediated by slow amplitude modulations between neighboring sites. These beat modes couple back to the phase dynamics via the amplitude dependent optical spring effect,  $\Omega(\bar{A}) + d\Omega \cdot (A - \bar{A})/\bar{A}$ , where  $d\Omega = \bar{A} \frac{d\Omega}{dA}|_{A=\bar{A}}$ , and the bare mechanical coupling  $K$ , leading to two opposing terms in  $K_1$ . Here,  $\bar{A}$  denotes the steady state mechanical amplitude and  $\gamma$  the amplitude decay rate set by the optical field. The fluctuating

noise force  $\sim \xi_\varphi$  comprises the effects of mechanical fluctuations and radiation pressure noise and is characterized by a diffusion constant  $D_\varphi$  [2, 29].

Equation (S.11) reveals the close connection to the Kuramoto model [3] and the two-dimensional xy-model. In the incoherent regime, the order parameter  $R$  is zero and the phase fluctuates freely. In the coherent regime, the restoring force  $\sim K_1 R$  leads the phase  $\varphi$  towards a fixed relation with  $\Psi$ . The cosine term only renormalizes the oscillation frequency. This statement can be clarified by a linear stability analysis, see [5, 29]. It turns out that the incoherent phase becomes unstable for

$$K_1 = 2D_\varphi, \quad (7)$$

defining the threshold of the transition. Moreover, if  $K_1$  becomes negative, no stable phase synchronization is possible. This situation arises if  $d\Omega < 0$ , or for large intercellular coupling rates  $K > 2d\Omega$ , see Fig. 3(d).

*Experimental prospects.* - We note that observation of the mechanical phase transition does *not* require single photon strong coupling ( $g_0 \gtrsim \kappa$ ): The quantum fluctuations of the light field will dominate over thermal fluctuations as long as  $4g_0^2|\alpha|^2/\kappa > k_B T/Q$ . This is essentially the condition for ground-state cooling, which has been achieved using high- $Q$  mechanical resonators and cryogenic cooling [14, 17], see Table I. In contrast, the photon-blockade effect (Fig. 2) requires low temperatures  $T$  and  $g_0^2 \gtrsim \Omega\kappa$ , or at least, in a slightly modified setup [35, 36],  $g_0 \gtrsim \kappa$ . While still challenging, optomechanical systems are approaching this regime [37].

Microfabricated optomechanical systems such as microresonators (e.g. [11]), optomechanical crystals (e.g. [17]) or microwave-based setups (e.g. [14]) lend themselves to extensions to optomechanical arrays. Here, we focus on optomechanical crystals, which are well suited due to their extremely small mode volumes. The properties of two-dimensional optomechanical crystals have been analyzed in [18]. The finite overlap of the evanescent tails of adjacent localized modes [29] results in a coupling of the form of Eq. (2), in analogy to the tight-binding description of electronic states in solids. Sufficiently strong optical and mechanical hopping rates are feasible, see [1] for one-dimensional and [29] for two-dimensional structures. The simultaneous optical driving of many cells

Setup	$T$ [K]	$\Gamma_{\text{nth}}/\Omega$	$\Gamma_{\text{opt}}/\Omega$	$g_0/\kappa$	$L$ [ $\mu\text{m}$ ]
Microwave based	25 mK	$10^{-4}$	$7 \times 10^{-3}$	$10^{-3}$	$\sim 100$
Optomech. crystal	20 K	$10^{-3}$	$4 \times 10^{-3}$	$2 \cdot 10^{-3}$	$\sim 4$
Microtoroid	650 mK	$7 \times 10^{-2}$	$6 \times 10^{-2}$	$5 \times 10^{-4}$	$\sim 30$

Table I. Parameters of optomechanical systems [11, 14, 17]: Temperature of phonon bath  $T$ , strength of mechanical fluctuations  $\Gamma_{\text{nth}} \approx k_B T/Q$ , strength of cavity shot noise  $\Gamma_{\text{opt}} \approx 4g_0^2|\bar{\alpha}|^2/\kappa$ , quantum parameter  $g_0/\kappa$  and approximate size  $L$ .

may be realized by a single broad laser beam irradiating the slab, see Fig. 1. Alternatively, similar physics may be observed for many mechanical modes coupling to one extended in-plane optical mode [1, 6, 25] (thereby effectively realizing global coupling).

The transition towards the synchronized phase can be detected by probing the light reflected from the optomechanical array and measuring the component oscillating at the mechanical frequency, see Fig. 3(d). To read out correlations between individual sites, the intensities of individual defect cavities may be analyzed [29], for example by evanescently coupling them to tapered fibers or waveguides.

We expect the transition to be robust against disorder [1]. One may also study the formation of vortices and other topological defects induced by engineered irregularities and periodic variations, and explore various different lattice structures or the possibility of other order phases (e.g. anti-ferromagnetic order). Thus, optomechanical arrays provide a novel, integrated and tunable platform for studies of quantum many body effects.

The authors would like to thank Oskar Painter and Björn Kubala for valuable discussions. This work was supported by the DFG Emmy-Noether program, an ERC starting grant, the DARPA/MTO ORCHID program and the ITN network cQOM.

---

\* max.ludwig@physik.uni-erlangen.de

- [1] J. D. Teufel, T. Donner, D. Li, J. W. Harlow, M. S. Allman, K. Cicak, A. J. Sirois, J. D. Whittaker, K. W. Lehnert, and R. W. Simmonds, *Nature* **475**, 359 (2011).
- [2] J. Chan, T. P. Mayer Alegre, A. H. Safavi-Naeini, J. T. Hill, A. Krause, S. Groblacher, M. Aspelmeyer, and O. Painter, *Nature* **478**, 89 (2011).
- [3] D. E. Chang, A. H. Safavi-Naeini, M. Hafezi, and O. Painter, *New J. Phys.* **13**, 023003 (2011).
- [4] M. Schmidt, M. Ludwig, and F. Marquardt, *New J. Phys.* **14**, 125005 (2012).
- [5] A. Tomadin, S. Diehl, M. D. Lukin, P. Rabl, and P. Zoller, *Phys. Rev. A* **86**, 033821 (2012).
- [6] A. Xuereb, C. Genes, and A. Dantan, *Phys. Rev. Lett.* **109**, 223601 (2012).
- [7] P. Rabl, *Phys. Rev. Lett.* **107**, 063601 (2011).
- [8] T. Carmon, H. Rokhsari, L. Yang, T. J. Kippenberg, and K. J. Vahala, *Phys. Rev. Lett.* **94**, 223902 (2005); Florian Marquardt, J. G. E. Harris, and S. M. Girvin, *ibid.* **96**, 103901 (2006); C. Metzger, M. Ludwig, C. Neuenhahn, A. Ortlieb, I. Favero, K. Karrai, and F. Marquardt, *ibid.* **101**, 133903 (2008); Q. Lin, J. Rosenberg, X. Jiang, K. J. Vahala, and O. Painter, *ibid.* **103**, 103601 (2009); M. Bagheri, M. Poot, M. Li, W. P. H. Pernice, and H. X. Tang, *Nat. Nanotechnol.* **6**, 726 (2011).
- [9] Z. Hadzibabic, P. Krüger, M. Cheneau, B. Battelier, and J. Dalibard, *Nature* **441**, 1118 (2006).
- [10] R. Fazio and H. van der Zant, *Physics Reports* **355**, 235 (2001).
- [11] S. Diehl, A. Micheli, A. Kantian, B. Kraus, H. P. Buchler, and P. Zoller, *Nat. Phys.* **4**, 878 (2008).
- [12] D. Nagy, G. Kónya, G. Szirmai, and P. Domokos, *Phys. Rev. Lett.* **104**, 130401 (2010).
- [13] K. Baumann, C. Guerlin, F. Brennecke, and T. Esslinger, *Nature* **464**, 1301 (2010).
- [14] T. E. Lee, H. Häffner, and M. C. Cross, *Phys. Rev. A*, **84**, 031402 (2011).
- [15] M. J. Hartmann, F. G. S. L. Brandão, and M. B. Plenio, *Nat. Phys.* **2**, 849 (2006).
- [16] A. D. Greentree, C. Tahan, J. H. Cole, and L. C. L. Hollenberg, *Nat. Phys.* **2**, 856 (2006).
- [17] D. E. Chang, V. Gritsev, G. Morigi, V. Vuletić, M. D. Lukin, and E. A. Demler, *Nat. Phys.* **4**, 884 (2008).
- [18] A. Nunnenkamp, K. Børkje, and S. M. Girvin, *Phys. Rev. Lett.* **107**, 063602 (2011).
- [19] A. Kronwald, M. Ludwig, and F. Marquardt, *Phys. Rev. A* **87**, 013847 (2013).
- [20] L. Mandel and E. Wolf, *Optical Coherence and Quantum Optics* (Cambridge University Press, Cambridge, England, 1995).
- [21] F. Nissen, S. Schmidt, M. Biondi, G. Blatter, H. E. Türeci, and J. Keeling, *Phys. Rev. Lett.* **108**, 233603 (2012).
- [22] M. Ludwig, B. Kubala, and F. Marquardt, *New J. Phys.* **10**, 095013 (2008);
- [23] J. Qian, A. A. Clerk, K. Hammerer, and F. Marquardt, *Phys. Rev. Lett.* **109**, 253601 (2012).
- [24] G. Heinrich, M. Ludwig, J. Qian, B. Kubala, and F. Marquardt, *Phys. Rev. Lett.* **107**, 043603 (2011).
- [25] C. A. Holmes, C. P. Meaney, and G. J. Milburn, *Phys. Rev. E* **85**, 066203 (2012).
- [26] M. Zhang, G. S. Wiederhecker, S. Manipatruni, A. Barnard, P. McEuen, and M. Lipson, *Phys. Rev. Lett.* **109**, 233906 (2012).
- [27] G. L. Giorgi, F. Galve, G. Manzano, P. Colet, and R. Zambrini, *Phys. Rev. A* **85**, 052101 (2012).
- [28] T. E. Lee and M. C. Cross, arXiv:1209.0742.
- [29] See Supplemental Material for details on the effective phase equations, possible experimental implementations and the numerical methods used.
- [30] A. Polkovnikov, *Ann. Phys.* **325**, 1790 (2010).
- [31] D. A. Rodrigues and A. D. Armour, *Phys. Rev. Lett.* **104**, 053601 (2010).
- [32] Y. Kuramoto, *Prog. Theor. Phys. Suppl.* **79**, 223 (1984).
- [33] S. H. Strogatz and R. E. Mirollo, *J. Stat. Phys.*, **63**, 613 (1991).
- [34] E. Verhagen, S. Deleglise, S. Weis, A. Schliesser, and T. J. Kippenberg, *Nature* **482**, 63 (2012).
- [35] K. Stannigel, P. Komar, S. J. M. Habraken, S. D. Bennett, M. D. Lukin, P. Zoller, and P. Rabl, *Phys. Rev. Lett.* **109**, 013603 (2012).
- [36] M. Ludwig, A. H. Safavi-Naeini, O. Painter, and F. Marquardt, *Phys. Rev. Lett.* **109**, 063601 (2012).
- [37] J. Chan, A. H. Safavi-Naeini, J. T. Hill, S. Meenehan, and O. Painter, *Appl. Phys. Lett.* **101**, 081115 (2012).
- [38] A. H. Safavi-Naeini and O. Painter, *Opt. Express* **18**, 14926 (2010).
- [39] A. H. Safavi-Naeini and O. Painter, *New J. Phys.* **13**, 013017 (2011).

# Supplemental Material for "Quantum many-body dynamics in optomechanical arrays"

Max Ludwig<sup>1,\*</sup> and Florian Marquardt<sup>1,2</sup>

<sup>1</sup>*Institute for Theoretical Physics, Universität Erlangen-Nürnberg, Staudtstraße 7, 91058 Erlangen, Germany*

<sup>2</sup>*Max-Planck-Institute for the Science of Light, Günther-Scharowsky-Straße 1/Bau 24, 91058 Erlangen, Germany*

## MEAN-FIELD PHASE EQUATION

In this section, we provide details for the derivation of the mean-field phase equation, Eq. (S.11), starting from the equations of motion of the optomechanical array, Eqs. (5). Introducing phases  $\varphi_j$  and amplitudes  $A_j$  (in units of the mechanical ground state width) as new coordinates of mechanical motion and omitting fast oscillating terms, the so-called Hopf equations are derived directly from (5). We follow [1], but add noise terms:

$$\begin{aligned}\dot{\varphi}_i &= -\Omega(A) + \frac{K}{zA_i} \sum_{\langle ij \rangle} A_j \cos(\varphi_j - \varphi_i) + \frac{\tilde{\xi}_\varphi}{A_i} \\ \dot{A}_i &= -\gamma(A_i - \bar{A}) - \frac{K}{z} \sum_{\langle ij \rangle} A_j \sin(\varphi_j - \varphi_i) + \tilde{\xi}_A\end{aligned}\quad (\text{S.8})$$

The steady amplitude  $\bar{A}$  and the amplitude decay rate  $\gamma$  are determined by the optical field:  $\gamma(A - \bar{A}) = (\Gamma + \Gamma_{\text{opt}}(A))A/2$ , where  $\Gamma_{\text{opt}} = -4g_0\langle|\alpha|^2 \sin\varphi\rangle_T$  and where  $\langle\dots\rangle_T$  denotes the average over one mechanical period. The mechanical oscillation frequency is modified via an amplitude dependent optical spring effect:  $\Omega(A) = \Omega - 2g_0\langle|\alpha|^2 \cos\varphi\rangle_T/A$ . The fluctuating noise forces  $\tilde{\xi}_\varphi$  and  $\tilde{\xi}_A$  comprise the effects of the phonon bath and the cavity shot noise, see [2] and below.

For weak coupling,  $K/z \ll \Omega$ , the fluctuations of the mechanical amplitudes around the steady state value  $\bar{A}$  are given by [1]

$$\delta A_i(t) \approx -\frac{K\bar{A}}{z\gamma} \sum_{\langle ij \rangle} \sin(\varphi_j(t) - \varphi_i(t)). \quad (\text{S.9})$$

These beat modes introduce an effective second order coupling between phases at different sites, as can be seen after plugging Eq. (S.9) into the Hopf equation for  $\varphi_i$  (S.8) and performing the time averages  $\langle\dots\rangle_T$ :

$$\begin{aligned}\dot{\varphi}_i &= -\Omega(\bar{A}) + \frac{K}{z} \sum_{\langle ij \rangle} \cos(\varphi_j - \varphi_i) + \frac{K}{z\gamma} \frac{d\Omega}{dA} \sum_{\langle ij \rangle} \sin(\varphi_j - \varphi_i) \\ &+ \frac{K^2}{2z^2\gamma} \sum_{\langle ij \rangle} \sum_{\langle jk \rangle} (\sin(2\varphi_j - \varphi_k - \varphi_i) - \sin(\varphi_k - \varphi_i)) \\ &+ \frac{K^2}{2z^2\gamma} \sum_{\langle ij \rangle} \sum_{\langle ik \rangle} \sin(\varphi_j + \varphi_k - 2\varphi_i) + \xi_\varphi,\end{aligned}\quad (\text{S.10})$$

where we introduced  $d\Omega = \bar{A} \frac{d\Omega}{dA} |_{A=\bar{A}}$ . This equation is similar to the xy model and the Kuramoto model in the

presence of noise, but with additional terms that mainly shift the frequency (the cos-term) and indicate higher-order coupling (the contributions of the double sums).

Ultimately, we apply a mean-field approximation: We replace  $e^{i\varphi_j}$  for neighboring cells by  $\langle e^{i\varphi_j} \rangle \equiv R e^{i\Psi}$  and  $e^{i2\varphi_j}$  by  $\langle e^{i2\varphi_j} \rangle \equiv R_2 e^{i\Psi_2}$ , where  $\langle\dots\rangle$  denotes the average over all sites [3], and arrive at the effective phase equation, Eq. (S.11), with additional second order contributions:

$$\begin{aligned}\dot{\varphi} &= -\Omega(\bar{A}) + KR \cos(\Psi - \varphi) + K_1 R \sin(\Psi - \varphi) \\ &+ K_2 R^2 \sin(2\Psi - 2\varphi) + K_2 R R_2 \sin(\Psi_2 - \Psi - \varphi) + \xi_\varphi,\end{aligned}\quad (\text{S.11})$$

where we introduced the effective coupling rates

$$K_1 = Kd\Omega/\gamma - K_2, \quad (\text{S.12})$$

$$K_2 = K^2/2z^2\gamma. \quad (\text{S.13})$$

## PHASE DIFFUSION

Here, we list some more details of the phase diffusion in the system based on the analysis given by Rodrigues and Armour [2] for a single optomechanical cell. The diffusion constant associated with  $\xi_\varphi$  (see Eq. (S.10)) is given by

$$D_\varphi = \frac{1}{A^2} (\tilde{D}_\varphi + \frac{\delta\Omega^2}{\gamma^2} \tilde{D}_A), \quad (\text{S.14})$$

where  $\tilde{D}_\varphi$  and  $\tilde{D}_A$  correspond to the noise acting on phase and amplitude in Eqs. (S.8), and where the diffusion rates are defined as

$$2\tilde{D}_{\varphi,A} = \int_{-\infty}^{\infty} d\tau \langle \tilde{\xi}_{\varphi,A}(t+\tau) \tilde{\xi}_{\varphi,A}(t) \rangle_T \quad (\text{S.15})$$

and likewise for  $D_\varphi$ . For the explicit expressions we refer to [2]. In the limit of  $g_0\bar{A} \ll \Omega$ , and for  $\Omega \gg \kappa$  and  $\Delta = \Omega$ , the maximum diffusion rates can be approximated by

$$2\tilde{D}_{\varphi,A} \approx \Gamma + \Gamma_{\text{opt}}, \quad (\text{S.16})$$

i.e. the sum of the intrinsic mechanical damping  $\Gamma$  and the optomechanical damping rate at the mechanical sideband

$$\Gamma_{\text{opt}} \approx 4g_0^2 |\bar{\alpha}|^2 / \kappa. \quad (\text{S.17})$$

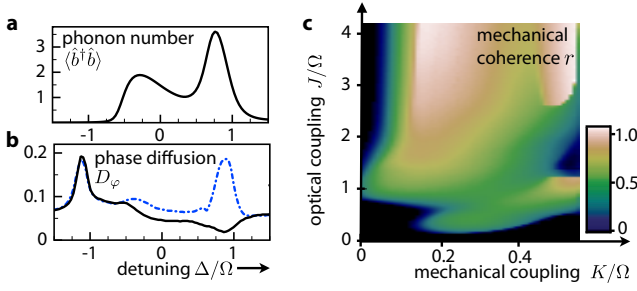


Figure S5. Additional details for the quantum dynamics of the optomechanical array within the mean-field approximation: (a) The phonon number  $\langle \hat{b}^\dagger \hat{b} \rangle$  shows, as a function of detuning, maxima at the resonance and at the sideband ( $\Delta \approx \Omega - g_0^2/\Omega$ ). (b) The diffusion constant for the mechanical phase,  $D_\varphi$ , for an uncoupled ( $K = 0$ , solid line) and a coupled array ( $K = 0.1\Omega$ , dash-dotted line). Other parameters as in Fig. 3. (c) Interplay of mechanical and optical coupling: Mechanical coherence is observed as a function of both mechanical and optical coupling.  $\Delta + J = \Omega/2$ , other parameters as in Fig. 2.

The diffusion of the mechanical phase can also be studied using the full quantum simulations and evaluating the linewidth of the correlator  $\langle \hat{b}(t)\hat{b}^\dagger(0) \rangle \sim e^{-(i\Omega_{\text{eff}} + D_\varphi)t}$ , see Fig. S5(b). Close to the onset, for small amplitudes  $\bar{A}$  and weak amplitude damping  $\gamma$ , the mechanical phases are very susceptible to quantum noise preventing synchronization. For finite coupling strengths, the diffusion is also enhanced, most strikingly at the mechanical sideband. As a result, the synchronization threshold shows a minimum between the onset of self-oscillations and the sideband, as observed in Fig. 3(a). From extended simulations, we find that this behavior is generic for systems in the resolved sideband regime ( $\Omega > \kappa$ ).

### STABILITY ANALYSIS

Here, we briefly recall details of the stability analysis leading to Eq. (7), which, for the case of the Kuramoto model, has been given in [4, 5]. We consider the density of the mechanical phases,  $\varrho(\varphi)$ . It is normalized,  $\int_0^{2\pi} \varrho(\varphi) d\varphi = 1$ , and the order parameter  $R$  and the mean-field  $\Psi$  can be computed from  $Re^{i\Psi} = \int_0^{2\pi} e^{i\varphi} \varrho(\varphi) d\varphi$  (and likewise for  $R_2$  and  $\Psi_2$ ). The Fokker-Planck equation corresponding to Eq. (S.11) is given by

$$\partial_t \varrho + \partial_\varphi (\varrho v) = D_\varphi \partial_\varphi^2 \varrho \quad (\text{S.18})$$

with a velocity

$$v = -\Omega(\bar{A}) + K \cos(\Psi - \varphi) + K_1 R \sin(\Psi - \varphi) + \mathcal{O}(R^2), \quad (\text{S.19})$$

where second order contributions can be neglected for this linear analysis. In the unsynchronized regime, the mechanical phases are equally distributed over the interval  $[0, 2\pi]$ , and  $\varrho = (2\pi)^{-1}$ . To study the time evolu-

tion of a small fluctuation on top of the incoherent background, we employ the ansatz [5]:

$$\varrho(\varphi) = \frac{1}{2\pi} + c(t)e^{i\varphi} + c^*(t)e^{-i\varphi}, \quad (\text{S.20})$$

leading to

$$\dot{c} = -\left(i\left(\Omega - \frac{K}{2}\right) + \left(D_\varphi - \frac{K_1}{2}\right)\right)c. \quad (\text{S.21})$$

This equation reveals that the incoherent solution  $\varrho = (2\pi)^{-1}$  becomes unstable for

$$K_1 = 2D_\varphi. \quad (\text{S.22})$$

and thus defines the coupling threshold for the synchronization transition [5].

### EXPERIMENTAL IMPLEMENTATION

(a) *Competing setups* - Here, we provide some details on possible experimental implementations suitable for observing the mechanical transition:

- Microdisks [6–8] and microtoroids [9–11] fabricated on microchips: Strong optical coupling between resonators is feasible via evanescent fields [8]. For both types of setups, scalability still has to be shown.
- Micro- and nanomechanical beams [12, 13] or membranes [14] coupling to superconducting microwave cavities: Mechanical interaction may be achieved via a common support or, capacitively, by applying a voltage bias between the mechanical resonators. Two-dimensional arrays of coupled microwave cavities are starting to be developed [15]. Related electromechanical systems (see, e.g., [16] for a setup comprising a nanobeam coupling to a superconducting single electron transistor) may also be employed.
- Optomechanical crystals [17–19] feature small mode volumes and are thus very suitable for extensions to optomechanical arrays. Some details of the proposed implementation are given below (Fig. S6).

(b) *Required parameters*: According to our semiclassical analysis, the essential requirement is

$$K\bar{A}^2 \gtrsim \Gamma_{\text{opt}} > \Gamma n_{\text{th}}. \quad (\text{S.23})$$

In this case, quantum noise ( $\Gamma_{\text{opt}}$ ) dominates over thermal fluctuations ( $\Gamma n_{\text{th}}$ ), which enter the model by replacing  $\Gamma \rightarrow \Gamma n_{\text{th}} \approx k_B T/Q$  in Eqs. (5). The mechanical transition can then be studied by varying  $\Gamma_{\text{opt}}$  via the laser detuning  $\Delta$ .

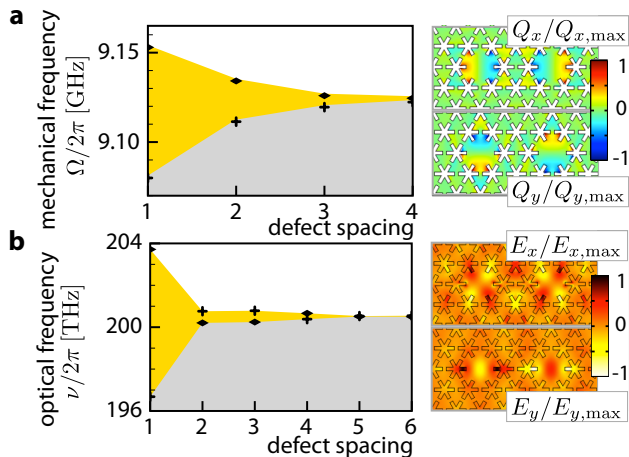


Figure S6. Variation of coupling strength with separation between defect cavities: (a) mechanical and (b) optical frequencies of symmetric (cross) and antisymmetric (diamond) normal modes for two defects on a snowflake optomechanical crystal (as discussed in the main text). The insets show the displacement field (electrical field) components of the antisymmetric mode for a defect separation of 2. The bare frequencies of the localized eigenmodes are 9.12 GHz and 200.5 THz, respectively. We note that the optical splittings (and likewise  $J$ ) change sign when varying the defect separation. Results obtained from finite element simulations.

Recent experiments have demonstrated  $\Gamma_{\text{opt}} > \Gamma_{\text{nth}}$ , see Table I. We note that two-dimensional optomechanical crystal devices are expected to show very good optomechanical properties [18], even exceeding those of existing one-dimensional setups [17].

(c) *Photon and phonon hopping amplitudes*: Using finite element simulations, we studied the hybridization of the photon and phonon modes of two defect cavities inside a two-dimensional snowflake silicon optomechanical crystal to obtain the hopping constants as a function of defect separation. Parameters: relative permittivity  $\epsilon_r = 11.68$ , Poisson ratio 0.17, density 2329 kg/m<sup>3</sup>, Young's modulus 170 GPa, snowflake design [20] with lattice constant 500 nm, snowflake radius 168 nm and snowflake width 60 nm. The mechanical and optical splittings (i.e. couplings  $2K/z$  and  $2J/z$ , respectively) reach values of up to 8% and 4% of the mechanical and optical eigenfrequencies, respectively (Fig. S6). These values are compatible with the requirements given by Eq. (S.23), even for very small oscillation amplitudes of the order of the mechanical zero-point width,  $\bar{A} \approx 1$ .

Other experimental approaches may realize different coupling terms, e.g.  $(\hat{x}_i - \hat{x}_j)^2$  [21]. Additional fast rotating terms like  $\hat{b}_i \hat{b}_j$  are, however, negligible for  $K/z \ll \Omega$ .

We note that the transition from incoherent to synchronized dynamics is also observable for extended optical modes ( $J \gg \Omega, \kappa$ ), see Fig. S5(c).

(d) *Optical drive*: In principle, the methods used for driving single defect modes via tapered and dimpled fibers [22] and optical waveguides [23, 24] can be extended to larger scales. To limit experimental efforts, however, one may drive the array using a freestanding broad laser beam, see the schematic picture in Fig. 1. The coupling between laser mode and the in-plane cavity modes will be relatively weak, which, however, can be compensated via the laser power. Preliminary experimental results on free space coupling to optomechanical crystals have been reported in [25].

(e) *Detection*: To detect the mechanical transition, measurements of the optical field emitted from the array are sufficient, see Fig. 3(d). To determine correlations between two separate lattice sites, the intensity emanating from these defect cavities may be probed by two tapered fibers in the near-field of the selected cells [22] or by especially designed waveguides [23, 24]. The correlations between the mechanical sideband components of the optical intensities  $\mathcal{I}_i(t) = \int_t^{t+2\pi/\Omega_{\text{eff}}} e^{i\Omega_{\text{eff}}t'} |\alpha_i|^2(t') dt'$ , are then proportional to the mechanical correlations,

$$\langle \mathcal{I}_i \mathcal{I}_j^* \rangle \propto \langle e^{i\varphi_i} e^{-i\varphi_j} \rangle. \quad (\text{S.24})$$

## NUMERICAL METHODS

To study the quantum dynamics of the system, we numerically integrate the Lindblad master equation (see main text) to the steady state (independent of initial conditions) using a fourth-order Runge-Kutta algorithm.

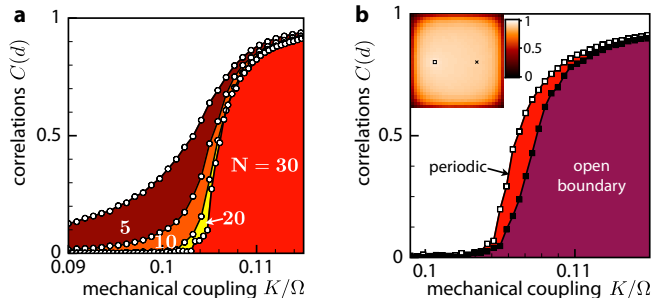


Figure S7. Langevin dynamics on finite square lattices, confirming results shown in Fig. 4: (a) Correlations  $C(d)$  as a function of coupling strength for different lattice sizes  $N \times N$  with  $N = \{5, 10, 20, 30\}$  ( $d = \{2, 4, 9, 14\}$ , periodic boundary conditions). (b) Correlations  $C(d = 14)$  on a  $30 \times 30$  square lattice with periodic boundary conditions (empty squares) and open boundary conditions (filled squares). The inset shows the correlations  $|\langle e^{i\varphi_i} e^{-i\varphi_j} \rangle|$  for  $i = (8, 15)$  (square) and  $K = 0.115$  and open boundary conditions. The cross marks the lattice site  $j = (22, 15)$  for which the correlations are shown in the main plot. Other parameters as in Fig. 4.

The size of the Hilbert space is optimized to enable an adequate representation of the physical state while obtaining reasonable simulation times. Typically, 10 – 20 photon and phonon levels, respectively, were taken into account. When slowly sweeping through parameter space, bistable behavior is revealed. This can be seen most prominently in Fig. S5(c) from the cut line in the right part of the plot.

The numerical integration of the Langevin equations (5) was obtained using a fourth order Runge-Kutta method for stochastic differential equations [26]. When evaluating the dependence of the threshold value on the quantum parameter  $g_0/\kappa$  (Fig. 4), the value of  $g_0\alpha_L$  was held constant. In this case, only the strength of quantum fluctuations changes (keeping the classical solution constant). For very large values of  $g_0/\kappa$ , fluctuations are overestimated by the Langevin equations and one has to rely on the exact quantum simulations.

The finite element simulations of Figs.1 and S6 were performed using COMSOL Multiphysics. We studied a hexagonal silicon slab with sides of length  $5.6\ \mu\text{m}$  and restricted our simulations to two space dimensions, i.e. in-plane elastic deformations and electromagnetic waves, see also [20]. Extended simulations in three dimensions have to be employed to analyze the coupling of the cavity modes to the out-of plane-modes.

---

\* max.ludwig@physik.uni-erlangen.de

- [1] G. Heinrich, M. Ludwig, J. Qian, B. Kubala, and F. Marquardt, *Phys. Rev. Lett.* **107**, 043603 (2011).
- [2] D. A. Rodrigues and A. D. Armour, *Phys. Rev. Lett.* **104**, 053601 (2010).
- [3] Y. Kuramoto, *Prog. Theor. Phys. Suppl.* **79**, 223 (1984).
- [4] H. Sakaguchi, *Prog. Theor. Phys.* **79**, 39 (1988).
- [5] S. H. Strogatz and R. E. Mirollo, *J. Stat. Phys.* **63**, 613 (1991).
- [6] P. E. Barclay, K. Srinivasan, O. Painter, B. Lev, and H. Mabuchi, *Appl. Phys. Lett.* **89**, 131108 (2006).
- [7] L. Ding, C. Baker, P. Senellart, A. Lemaitre, S. Ducci, G. Leo, and I. Favero, *Phys. Rev. Lett.* **105**, 263903 (2010).
- [8] M. Zhang, G. S. Wiederhecker, S. Manipatruni, A. Barnard, P. McEuen, and M. Lipson, *Phys. Rev. Lett.* **109**, 233906 (2012).
- [9] D. K. Armani, T. J. Kippenberg, S. M. Spillane, and K. J. Vahala, *Nature* **421**, 925 (2003).
- [10] A. M. Armani, A. Srinivasan, and K. J. Vahala, *Nano Lett.* **7**, 1823 (2007).
- [11] E. Verhagen, S. Deleglise, S. Weis, A. Schliesser, and T. J. Kippenberg, *Nature* **482**, 63 (2012).
- [12] C. A. Regal, J. D. Teufel, and K. W. Lehnert, *Nat. Phys.* **4**, 555 (2008).
- [13] T. Rocheleau, T. Ndukum, C. Macklin, J. B. Hertzberg, A. A. Clerk, and K. C. Schwab, *Nature* **463**, 72 (2010).
- [14] J. D. Teufel, T. Donner, Dale Li, J. W. Harlow, M. S. Allman, K. Cicak, A. J. Sirois, J. D. Whittaker, K. W. Lehnert, and R. W. Simmonds, *Nature* **475**, 359 (2011).
- [15] A. A. Houck, H. E. Tureci, and J. Koch, *Nat. Phys.* **8**, 292 (2012).
- [16] A. Naik, O. Buu, M. D. LaHaye, A. D. Armour, A. A. Clerk, M. P. Blencowe, and K. C. Schwab, *Nature* **443**, 193 (2006).
- [17] J. Chan, T. P. Mayer Alegre, A. H. Safavi-Naeini, J. T. Hill, A. Krause, S. Groblacher, M. Aspelmeyer, and O. Painter, *Nature*, **478**, 89 (2011).
- [18] A. H. Safavi-Naeini and O. Painter, *Opt. Express* **18**, 14926 (2010).
- [19] E. Gavartin, R. Braive, I. Sagnes, O. Arcizet, A. Beveratos, T. J. Kippenberg, and I. Robert-Philip, *Phys. Rev. Lett.* **106**, 203902 (2011).
- [20] A. H. Safavi-Naeini and O. Painter, *New J. Phys.* **13**, 013017 (2011).
- [21] M. L. Roukes and E. Buks, *Journal of Microelectromechanical Systems* **11**, 6 (2002).
- [22] C. P. Michael, M. Borselli, T. J. Johnson, C. Chrystal, and O. Painter, *Opt. Express* **15**, 4745 (2007).
- [23] A. H. Safavi-Naeini, S. Groblacher, J. T. Hill, J. Chan, M. Aspelmeyer, and O. Painter, *Nature* **500**, 185 (2013).
- [24] J. D. Cohen, S. Meenehan, and O. Painter, *Opt. Express* **21**, 11227 (2013).
- [25] J. Chan, PhD thesis, California Institute of Technology, 2012.
- [26] N.J. Kasdin, *Proceedings of the IEEE*, **83**, 802 (1995).